Journal of Materials Chemistry

Cite this: *J. Mater. Chem.*, 2012, **22**, 16582

www.rsc.org/materials

PAPER

Molecular length adjustment for organic *azo*-based nonvolatile ternary memory devices†

Shifeng Miao,[a] Hua Li,[a] Qingfeng Xu,[a] Najun Li,[a] Junwei Zheng,[b] Ru Sun,[a] Jianmei Lu*[a] and Chang Ming Li[cd]

Received 11th May 2012, Accepted 8th June 2012
DOI: 10.1039/c2jm32992a

Two conjugated small molecules with different molecular length, **DPAPIT** and **DPAPPD**, in which an electron donor dimethylamino moiety and an electron acceptor phthalimide core unit are bridged by another electron-accepting azobenzene block, were designed and synthesized. **DPAPIT** molecule with longer conjugation length stacked regularly in the solid state and formed uniform nanocrystalline film. The fabricated memory devices with **DPAPIT** as active material exhibited outstanding nonvolatile ternary memory effect with the current ratio of $\sim 1 : 10^{1.7} : 10^{4}$ for "0", "1" and "2" states and all the switching threshold voltages lower than −3 V. In contrast, the shorter molecule **DPAPPD** showed amorphous microstructure and no obvious conductive switching behavior was observed in the device. The crystallinity and surface roughness of **DPAPIT** thin films were significantly improved as the annealing temperature increased, lowering the switching threshold voltages which are highly desirable for low-power consumption data-storage devices. It is worth noting that the tristable memory signals of **DPAPIT** film could also be achieved by using conductive atomic force microscopy with platinum-coated probe, which enables fabrication of nano-scale or even molecular-scale device, a significant progress for the ultra-high density data storage application. Mechanism analysis demonstrated that two charge traps with different depth in the molecular backbone were injected by charge carriers progressively as the external bias increased, resulting in the formation of three distinct conductive states (OFF, ON1 and ON2 states).

Introduction

Can you imagine that the whole database of U.S. library is stored in a stamp-sized chip? It could be done when the data-storage density is higher than 10^{12} bit per cm^2 which is still a big challenge for present optical or magnetic storage systems.[1–4] Organic electronic memory (OEM) based on polymeric or composite materials, has evoked considerable research interests due to its ability of 3D-stacked cross-bar array to realize ultra-high density data storage (UHDDS).[5–20] However, the fabrication process of 3D-stacked device is complex and time-consuming. Increasing the data storage states from binary to ternary is an easier way to achieve UHDDS which has "0", "1" and "2" tristable states and offers a unique opportunity to store more than 2-bits in a single cell, thereby achieving a high density memory with minimized downscaling.[21,22] To date, these ternary memory materials are still less-explored. Due to the designable molecular structures and less batch-to-batch variation in properties,[23] small organic molecules are promising alternatives to achieve high-performance device and have been widely studied in organic field-effect transistors,[24,25] light-emitting diodes,[26–28] and solar cells.[29–31] Their controllable π–π stacking style in the solid film facilitates the charge transport process and thus improves the electrical properties. Owing to these merits of small molecules, our group have successfully fabricated a small-molecule-based ternary OEM device through introducing different electron-deficient moieties into the conjugated molecular backbone.[22] Although much attention is being focused on designing new organic materials to obtain ternary data storage device, the ideal candidate should also be stable in ambient conditions, and possess high charge mobility to achieve low power consumption.

In this work, we present two small molecules with different molecular length 1-(4-((4-(dimethylamino)phenyl)diazenyl)-phenyl)-1*H*-pyrrole-2,5-dione (**DPAPPD**) and 2,6-bis(4-((4-(dimethylamino)phenyl)diazenyl)phenyl)pyrrolo[3,4-*f*]iso-indole-1,3,5,7-(2*H*,6*H*)-tetraone (**DPAPIT**), as shown in Scheme 1. Both molecules have an electron-donating dimethylamino moiety and an electron-accepting phthalimide core unit which are bridged by

[a]*Key Laboratory of Organic Synthesis of Jiangsu Province, College of Chemistry, Chemical Engineering and Materials Science, Soochow University, Suzhou, Jiangsu 215123, China. E-mail: lujm@suda.edu.cn; Fax: +86 512 65880367; Tel: +86 512 65880368*
[b]*Institute of Chemical Power Sources, Soochow University, Suzhou, Jiangsu 215006, China*
[c]*School of Chemical and Biomedical Engineering, Nanyang Technological University, 70 Nanyang Drive, 637457, Singapore*
[d]*Institute for Clean Energy and Advanced Materials, Southwest University, Chongqing 400715, China*

† Electronic supplementary information (ESI) available. See DOI: 10.1039/c2jm32992a

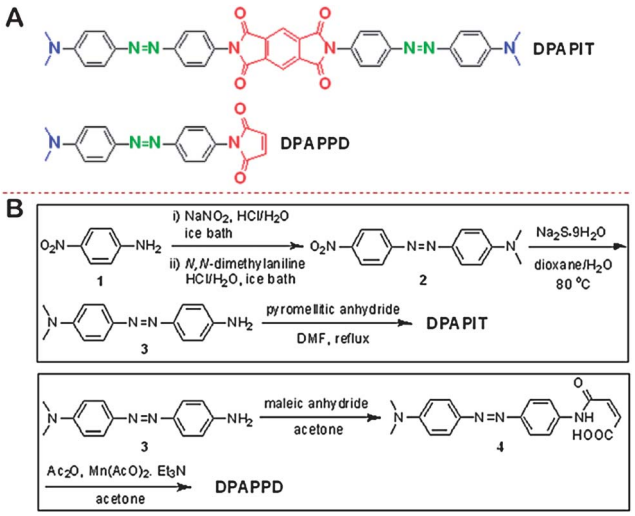

Scheme 1 (A) Chemical structure and (B) synthetic routes of **DPAPIT** and **DPAPPD**.

another electron-accepting azobenzene block. The influences of molecular length, film morphology, and annealing temperature on the memory device performance have been precisely and systematically investigated. The results showed that the sandwich memory device with the longer molecule (**DPAPIT**) as active layer exhibited excellent ternary electrical conductance switching and nonvolatile memory effects with long-term thermal stability. The shorter molecule (**DPAPPD**) showed poor memory performance and no conductance switching characteristics under the identical test conditions. Most importantly, the ternary memory signals could also be written and read out using conductive atomic force microscopy (C-AFM) tip onto the nano thin-film, which enables fabrication of nano-scale or even molecular-scale device. It would be a further step towards realizing UHDDS device.

Experimental

Materials

4-Nitroaniline, sodium nitrite, *N*,*N*-dimethylaniline, sodium sulfide, pyromellitic anhydride and maleic anhydride were purchased from commercial sources (TCI, Alfa Aesar, and Sigma-Aldrich). All solvents were purchased from Sinopharm Chemical Reagent Co., Ltd. All chemicals were used as received without further purification.

Preparation of DPAPIT and DPAPPD

DPAPIT and **DPAPPD** were synthesized successively by diazotization-coupling, reduction and condensation reactions in good yields as shown in Scheme 1. **DPAPIT** has almost twice the conjugation length of **DPAPPD**.

***N*,*N*-dimethyl-4-((4-nitrophenyl)diazenyl)aniline (2).** 4-Nitroaniline **1** (2.76 g, 20.0 mmol) was partially dissolved in a mixture of deionized water (8 mL) and concentrated aqueous HCl (8 mL) under heating in a water bath. The mixture was cooled by pouring it into ice water. After extended cooling in an ice bath, a solution of sodium nitrite (1.38 g, 20.0 mmol) in deionized water (5 mL) was added; the mixture became homogeneous. After 1 h, an ice-cold solution of *N*,*N*-dimethylaniline (2.42 g, 20.0 mmol) in a mixture of deionized water (20 mL) and concentrated aqueous HCl (4 mL) were added dropwise for 30 min at 0–5 °C. After stirring in ice-water bath for 2 h, the mixture was neutralized with proper amount of 1 M KOH solution. The mixture was filtered and washed with deionized water. The red powder was dried in the vacuum oven overnight at 60 °C. Yield of **2** is 89%.

4-((4-Aminophenyl)-diazen-yl)-*N*,*N*-dimethyl-aniline (3).[32,33] To a solution of **2** (0.54 g, 2.0 mmol) in dioxane (20 mL), $Na_2S \cdot 9H_2O$ (1.58 g, 6.6 mmol) in of H_2O (5 mL) was added in portions. The mixture was heated at 80 °C and stirred under nitrogen atmosphere until the thin-layer chromatography (TLC) showed no starting material **2**. The mixture was cooled to room temperature, then poured into water. After standing for 2 h, the mixture was filtered and washed with deionized water. The crude product was dried in the vacuum oven and purified by recrystallization from 50% ethanol to afford **3** as brown solid (0.37 g, 77%). ^{1}H NMR (400 MHz, DMSO-d_6) δ (ppm): 7.65 (d, J = 9.1 Hz, 2H), 7.55 (d, J = 8.7 Hz, 2H), 6.79 (d, J = 9.1 Hz, 2H), 6.63 (d, J = 8.8 Hz, 2H), 5.78 (s, 2H), 3.01 (s, 6H).

2,6-Bis(4-((4-(dimethylamino)phenyl)diazenyl)-phenyl)-pyrrolo[3,4-*f*]iso-indole-1,3,5,7-(2*H*,6*H*)-tetraone (DPAPIT). Reduction product **3** (0.30 g, 1.25 mmol) was dissolved in dimethylformamide (DMF, 5 mL). A solution of pyromellitic anhydride (0.14 g, 0.63 mmol) in DMF (4 mL) was added dropwise into it. After being refluxed for 12 h, the reaction mixture was cooled down to room temperature and poured into water. The precipitate was filtered and washed with water. Crude **DPAPIT** was obtained and purified by column chromatography on silica gel with ethyl acetate-petroleum ether as the eluent, yield 33%. ^{1}H NMR (400 MHz, DMSO-d_6) δ (ppm): 10.44 (s, 2H, ArH), 8.33 (s, 1H, ArH), 7.78–7.72 (m, 11H, ArH), 6.82 (d, J = 9.0 Hz, 4H, ArH), 3.05 (s, 12H, 4× CH_3). HRMS: calcd for $C_{38}H_{30}N_8O_4$ $[M + H]^+$ 663.2390, found 663.4539. Anal. calcd for $C_{38}H_{30}N_8O_4$: C, 68.87; H, 4.56; N, 16.91; found: C, 68.69; H, 4.48; N, 16.78%.

1-(4-((4-(Dimethylamino)phenyl)diazenyl)phenyl)-1*H*-pyrrole-2,5-dione (DPAPPD). Compound **3** (0.48 g, 2.0 mmol), maleic anhydride (0.20 g, 2.0 mmol) and acetone (10 mL) were added to a single-necked flask. After stirring for 8 h at 60 °C, intermediate product **4** was precipitated and collected by filtration. The filter cake was washed with ethyl acetate and dried under infrared lamp. Crude **4** was directly used in the next step without further purification. Compound **4**, triethylamine (0.19 g, 2.4 mmol) and acetone (10 mL) were stirred for 5 min at 60 °C. After dissolution of reactants, acetic anhydride (1.21 g, 11.6 mmol) and manganese acetate (0.01 g, as catalyst) were added and the mixture was continued to stir for 4 h at 60 °C. The reaction mixture was cooled to room temperature, then was poured into a large amount of water and isolated by filtration, the final yellow product was recrystallized from 95% ethanol. Yield of **DPAPPD**: 0.52 g, 78%. ^{1}H-NMR (400 MHz, DMSO-d_6), δ (ppm): 7.87 (d, J = 8.6 Hz, 2H, ArH), 7.81 (d, J = 8.6 Hz, 2H, ArH), 7.50 (d, J = 8.3 Hz, 2H, ArH), 7.23 (s, 2H, CHCO), 6.85 (d, J = 8.8 Hz,

2H, ArH), 3.07 (s, 6H, 2 × CH_3). HRMS: calcd for $C_{18}H_{16}N_4O_2$ $[M + H]^+$ 321.1273, found 321.1347. Anal. calcd for $C_{18}H_{16}N_4O_2$: C, 67.49; H, 5.03; N, 17.49; found: C, 67.55; H, 4.92; N, 17.39%.

Fabrication of the memory device

The indium-tin-oxide (ITO) glass was precleaned with water, acetone, and alcohol sequentially in an ultrasonic bath for 20 min. The active organic film was deposited under high vacuum ($\sim 10^{-6}$ Torr). The film thickness was about 80 nm. An aluminum (Al) layer with thickness of about 100 nm was thermally evaporated and deposited onto the organic surface at about 5×10^{-6} Torr through a shadow mask to form the top electrode. An active device area of ~ 0.0314 mm^2 was obtained.

Measurement

All electrical measurements of the device were characterized under ambient conditions without any encapsulation using an HP 4145B semiconductor parameter analyzer equipped with an HP 8110A pulse generator. NMR spectra were obtained from an Inova 400 MHz FT-NMR spectrometer. High-resolution mass spectra (HRMS) were determined on Micromass GCT-TOF mass spectrometer with ESI resource. Elemental analysis was performed using a Carlo-Erba EA-1110 instrument. UV-Vis absorption spectra were measured at room temperature by using a Shimadzu UV-3600 spectrophotometer. Cyclic voltammetry was performed at room temperature using an ITO working electrode, a reference electrode Ag/AgCl, and a counter electrode (Pt wire) at a sweep rate of 100 mV s^{-1} (CorrTest CS Electrochemical Workstation analyzer). A 0.1 M solution of tetrabutylammonium perchlorate (TBAP) in anhydrous DMF was used. Scanning electron microscopy (SEM) images were taken on a Hitachi S-4700 scanning electron microscope. Atomic force microscopy (AFM) measurements were performed by using a MFP-3DTM (Digital Instruments/Asylum Research) AFM instrument.

Results and discussion

Optical properties

As shown in Fig. 1a, the UV-Vis absorption spectrum of **DPAPIT** in dilute tetrahydrofuran (THF) solution displays a π–π* transition of the azobenzene chromophore at 320 nm (ref. 34–36) and a stronger intramolecular charge transfer (CT) transition at 481 nm.[35] We also measured the UV-Vis absorption spectrum of the vacuum-deposited thin films of **DPAPIT** on ITO substrate. Compared with the absorption spectrum in solution state, both the π–π* transition of the azobenzene segment and the charge transfer (CT) transition absorption peaks are obviously bathochromic-shifted (from 320 to 335 nm, and from 481 to 501 nm) and significantly broadened. Besides, absorbance in the longer wavelength region of the thin films increased with the increasing annealing temperatures (ESI, Fig. S1†). The red-shift and broadened absorption peaks from solution to solid state might be associated with the formation of molecular aggregation or orderly π–π stacking and/or increased polarizability of the film,[37,38] which is beneficial for improving the charge carrier mobility of the films. However, no evident difference was observed between the solution and film of the UV-Vis absorption spectra of the "counterpart" molecule **DPAPPD**, which indicates that this short molecule has poor capacity to stack orderly in the film state (ESI, Fig. S2†). The optical band gaps (E_g^{opt}) of **DPAPIT** at various annealing temperatures, determined from the onset of optical absorbance, are summarized in Table 1.

Electrochemical properties

Fig. 1b shows the cyclic voltammograms (CVs) of **DPAPIT** films on ITO glasses annealed at various temperatures using a 0.1 M solution of tetrabutylammonium perchlorate (TBAP) in anhydrous DMF. The onset oxidations (E_{ox}^{onset}) are ~0.95, 0.93, 0.91 and 0.90 V for films annealing at room temperature, 60 °C, 80 °C and 100 °C, respectively. The electrochemical potentials were measured using Ag/AgCl as a reference electrode. The external ferrocene/ferrocenium (F_c/F_c^+) redox standard potential ($E_{ferrocene}^{1/2}$) was measured to be 0.55 V *vs.* Ag/AgCl in DMF. Assuming that the HOMO level for the F_c/F_c^+ standard is −4.80 eV with respect to the zero vacuum level, the HOMO and LUMO levels for the **DPAPIT** films at different annealing temperatures are estimated. The detailed results are shown in Table 1.

The HOMO and LUMO energy levels of the **DPAPIT** and the work functions (Φ) of Al top and ITO bottom electrodes were compared to understand the memory behavior of **DPAPIT** based devices. The energy barrier between Φ of the ITO (−4.8 eV) and HOMO energy level is 0.35–0.41 eV, which is much lower than the energy barrier of 1.21–1.39 eV between the Φ of the Al (−4.3 eV) and LUMO energy level. This suggests that hole injection from ITO into the HOMO of **DPAPIT** (corresponding to ITO as the anode) is easier than electron injection from Al into the LUMO of **DPAPIT**. Thus, **DPAPIT** is a p-type material and holes predominate the conduction process (as shown in the inset of Fig. 1b).

Morphology of the thin films

Atomic force microscopy (AFM) was used to characterize the surface morphology of the vacuum-deposited electroactive layers. As shown in Fig. 2a, the tapping-mode AFM height images clearly show that **DPAPIT** formed two-dimensional grains in its solid state at room temperature with uniform size and minor roughness. This type of grain-like morphology has also been observed on other substrates having different polarities (*e.g.*, glass, silicon oxide and quartz), indicating that the intermolecular interactions is the driving force to self-assemble during the vapor-deposition process. However, only amorphous structures were observed for the "counterpart" compound **DPAPPD**, which might be due to relatively weak intermolecular π–π stacking interactions (ESI, Fig. S3†). As generally observed from organic semiconductors, AFM images revealed that the grain size increases with the increasing annealing temperatures (Fig. 2a–d). However, **DPAPPD** film still showed non-crystalline topography even after annealing at 60 °C or 90 °C. The XRD patterns of **DPAPIT** films deposited onto ITO glasses at different annealing temperatures are shown in Fig. 3. It exhibited an unconspicuous diffraction peak at $2\theta = 25°$ at room temperature

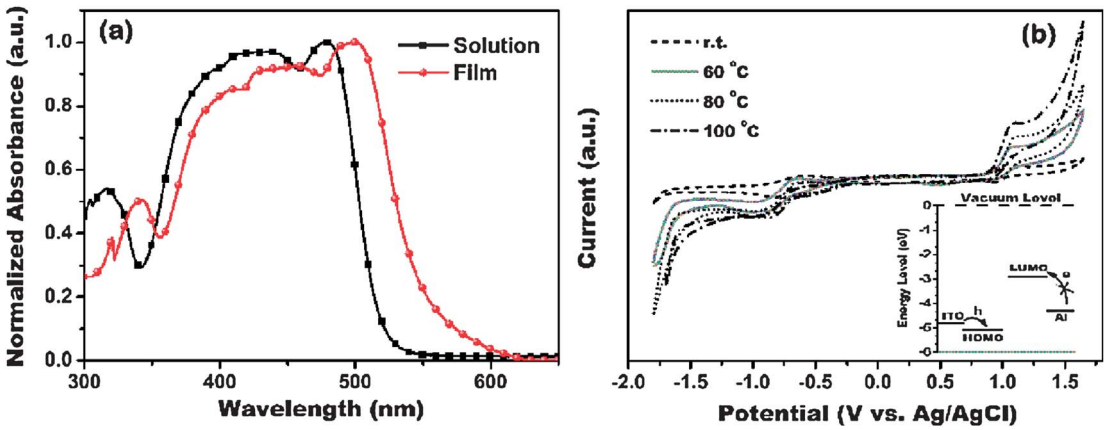

Fig. 1 (a) UV-Vis absorption spectra of **DPAPIT** in dilute THF solution and solid thin film on ITO substrate; (b) cyclic voltammograms of **DPAPIT** on a ITO electrode annealed at various temperatures in 0.1 M TBAP/DMF solution with Ag/AgCl as reference electrode and Pt wire as counter electrode. A scan rate of 100 mV s^{-1} was used. The inset shows HOMO and LUMO energy level of **DPAPIT** film annealing at 80 °C and work function of ITO and Al.

and a higher intensity peak at higher annealing temperatures. This value corresponds to a *d* spacing of 3.6 Å, a typical intermolecular π–π interaction distance. Another peak at $2\theta = 17°$ gradually appeared as the annealing temperature increased. These results indicate that the **DPAPIT** molecules self-assembled into highly ordered crystalline and packed closely in the thin film state. In contrast, no discernible XRD peak was observed for **DPAPPD** thin film deposited onto the same substrate, indicating an amorphous feature (ESI, Fig. S4†).

Current–voltage (*I–V*) characteristics

A schematic sandwich structure comprising of a pair of electrodes and a layer of small molecules is shown in Fig. 4a. *Azo* molecules were vapor-deposited onto an indium-tin oxide (ITO) substrate (~40 nm) at 2.0×10^{-4} Pa. The film thickness was ~80 nm, as measured by scanning electron microscopy (SEM) through a cross-section of the device (insert in Fig. 4a). Subsequently, Al top electrodes (0.2 mm diameter and near 100 nm thickness) were thermally deposited onto the film through a shadow mask. Fig. 4b shows the *I–V* curves of the organic memory devices, with **DPAPIT** thin films annealed at 80 °C as electroactive layer. In the first sweep from 0 to −3.0 V, two abrupt current increases were observed at switching threshold voltages around −1.50 V and −2.18 V, indicating that the device underwent sharp electrical transitions from a low-conductivity state ("0" or OFF state) to an intermediate-conductivity state ("1" or ON1 state) and then to a high-conductivity state ("2" or ON2 state). After the subsequent scan from 0 to −3 V, the storage cell remained in its high-conductivity state (sweep 2). Sweep 3 was to measure another cell of the device over a voltage range of 0 to −2.0 V and it showed a switching threshold voltage at −1.50 V. The intermediate-conductivity state ("1") could be maintained during the subsequent scan from 0 to −2.0 V even after removing the power supply (sweep 4). This device, therefore, exhibits a typical nonvolatile WORM (write-once, read-many-times) memory behavior. The transition from "OFF" to "ON1" state and then to "ON2" state can be regarded as the "writing" process for the memory devices. It should also be emphasized that our device is highly stable after proper data writing and that a constant voltage (−1.0 V, for example) can be employed to read the "0", "1" and "2" signals of the memory device (Fig. 4c). There is no significant degradation in any of the three states for almost ten hours. Furthermore, the effect of continuous read pulses of −1 V on the OFF, ON1 and ON2 states was also investigated (Fig. 4d). No obvious degradation in the current was observed for all the three states after more than one hundred million (10^8) continuous read cycles, indicating that any of the states was insensitive to the read pulses. The three states of the ternary memory cells are very distinct, with the current ratio of "0", "1" and "2" being ~1 : $10^{1.7}$: 10^4. In addition, the switching threshold voltages are all lower

Table 1 Optical and electrochemical properties of the **DPAPIT** films annealed at different temperatures

Annealing temp. (°C)	Film (nm) λ_{max}	E_g (eV)[b] λ_{onset}	E_{ox}^{onset} (V)[c]	HOMO[d] (eV)	LUMO (eV)	
r.t.[a]	479	541	2.29	0.95	−5.20	−2.91
60	484	551	2.25	0.93	−5.18	−2.93
80	494	564	2.20	0.91	−5.16	−2.96
100	501	569	2.18	0.90	−5.15	−2.97
120	505	585	2.12	0.96	−5.21	−3.09

[a] Room temperature is abbreviated as r.t. [b] The data were calculated by the following equation: bandgap = $1240/\lambda_{onset}$ of **DPAPIT** films at different annealing temperatures. [c] *Vs.* Ag/AgCl in anhydrous DMF. [d] The HOMO energy levels were calculated from cyclic voltammetry and were referenced to ferrocene (4.8 eV).

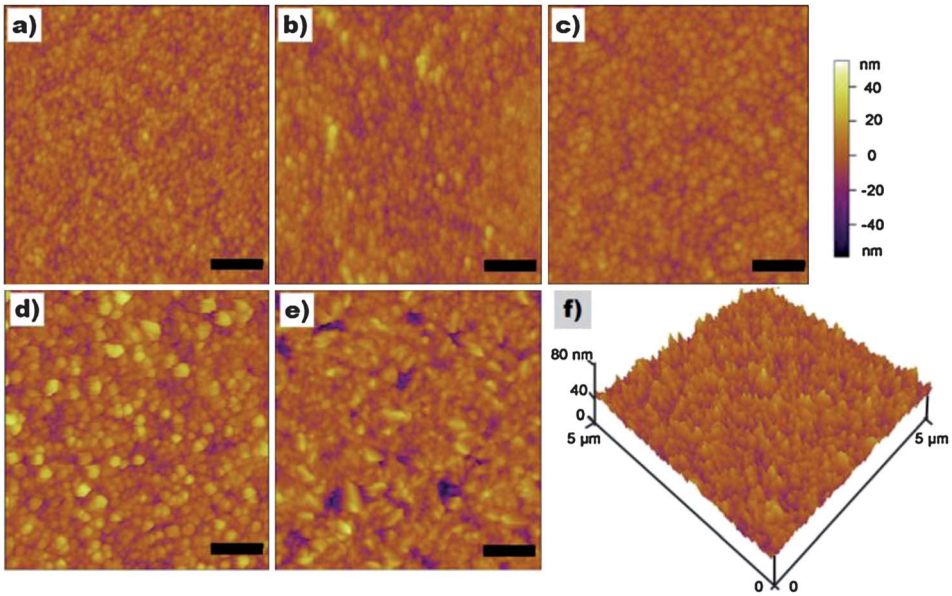

Fig. 2 Tapping-mode AFM height images of **DPAPIT** thin films vacuum-deposited onto ITO substrates annealed at different temperatures: (a) 25 °C, (b) 60 °C, (c) 80 °C, (d) 100 °C, and (e) 120 °C, respectively. Scale bars are equal to 1 μm. The color bar of the AFM images has been displayed in the right of (c). And (f) is corresponding to 3D-AFM topography image of (c).

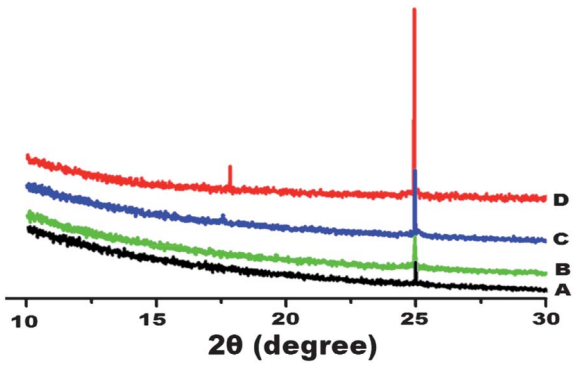

Fig. 3 XRD patterns of the vacuum-deposited **DPAPIT** thin films annealed at different temperatures for 12 hours: (A) without annealing; (B) 60 °C; (C) 80 °C; (D) 100 °C, respectively.

than −3 V and the read voltage is only −1 V, which indicates the ternary device has low power consumption and can be a promising candidate for portable electronic device in the future. The *I–V* curves of the "counterpart" molecule **DPAPPD** was also measured under the identical conditions. However, no abrupt current change was observed as the voltage scanned from 0 to −3 V (ESI, Fig. S5†), which can be ascribed to the disordered molecular packing within the amorphous films.

We also explored the effect of the film annealing temperatures on data storage properties. All the devices fabricated with **DPAPIT** films prepared under annealing temperature ranging from 25 to 100 °C exhibited excellent ternary data storage performances. The switching threshold voltage of the devices became lower as the annealing temperature increased (ESI, Fig. S6†). As can be seen from Fig. 5, the energy barrier of hole injection (ΔE, $\Phi_{ITO} - E_{HOMO}$) follow closely with the corresponding turn-on threshold voltages: both decreased gradually with increased annealing temperatures. These results further confirm that the charge conduction process of the ternary memory device is mainly dominated by the hole injection. The increasing annealing temperature helped to improve the film morphology and mobility of the charge carriers. However, as the annealing temperature reached 120 °C, the tristable switching performance was apparently affected, which is partly due to increased empty space between the grains and crack formation in the films upon cooling (Fig. 2e).[38–40] The influence of annealing temperatures on the *I–V* performance of the "counterpart" molecule **DPAPPD** has also been investigated. However, no sharp current changes could be observed at all the annealing temperatures (ESI, Fig. S5†).

C-AFM measurement

A C-AFM probe was used to perform the morphology scan onto the **DPAPIT** film (ITO as the bottom electrode) under various applied voltages, which is equivalent to writing different storage states into the film (the different areas with various scanning voltages are marked in Fig. 6a). After the writing process, the conductive tip with voltages −1 V, −4 V and −6 V were used to successively scan the recorded film to read out the electrical signals (Fig. 6a). Three distinct conducting states could be successfully read out, representing "0", "1" and "2" signals, respectively. Fig. 6b shows the 3D graph corresponding to Fig. 6a, from which we can clearly see different current responses marked as distinct storage states. The current values along the red line in Fig. 6a were shown in Fig. 6c. The currents of three conductive states were equal to the results from the bulk sandwich device mentioned above. With the aid of C-AFM tip, **DPAPIT** molecules can be used to fabricate nano-scale or even molecular-scale device, which would further improve the data-storage density.

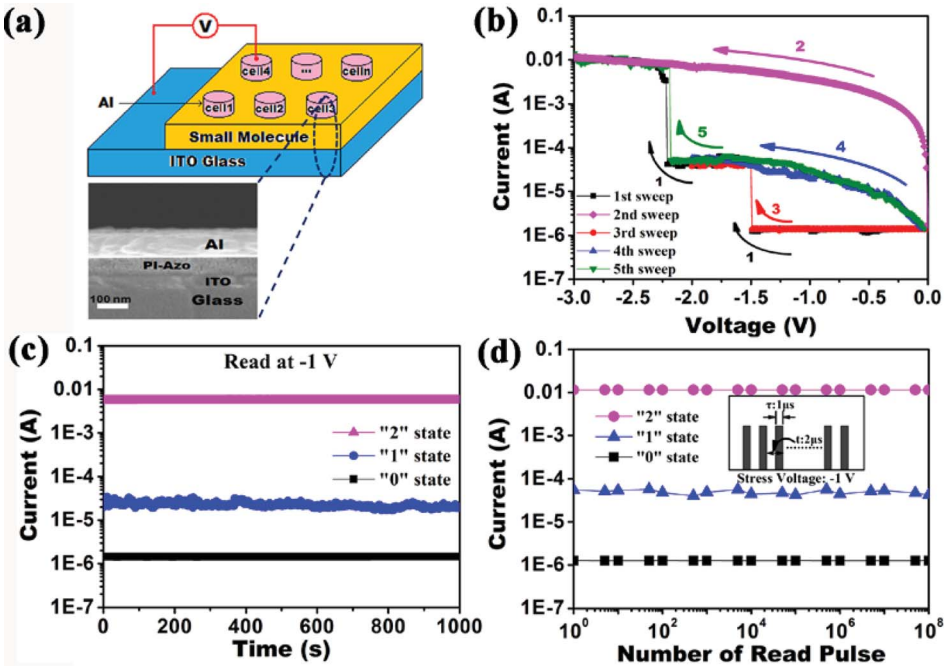

Fig. 4 (a) (top) Illustration of the sandwich device; (bottom) SEM image of a cross-section view of the device; (b) current–voltage (*I–V*) characteristics of the memory device fabricated with **DPAPIT** film annealed at 80 °C; (c) stability of the device in three states under a constant "read" voltage of −1 V; and (d) effect of read cycles on three states under a stress of voltage of −1 V.

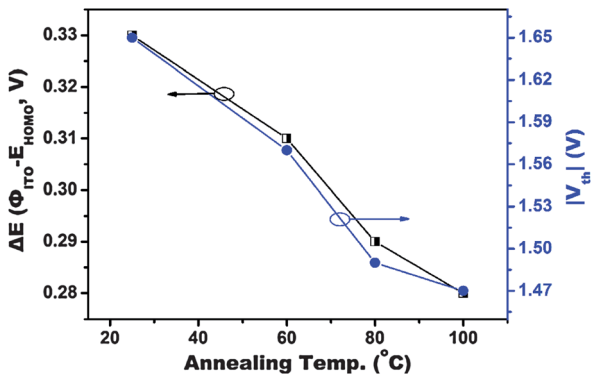

Fig. 5 The changes of the energy barrier of hole injection (ΔE, $\Phi_{ITO} - E_{HOMO}$) (black dot-and-line) and absolute threshold voltage ($|V_{th}|$) of the **DPAPIT**-based memory device (blue dot-and-line) with annealing temperatures.

Proposed data-storage mechanism

It was previously reported that the electrical switching of some polymeric thin films originated from the formation of metallic filaments spanning the entire polymer layer or native Al_2O_3 layer between the Al electrode and polymer layer.[41] In order to probe the possibility of filament formation, the freshly prepared **DPAPIT** film vacuum-deposited onto ITO were employed using the C-AFM tip which was coated with metallic Pt as the top electrode for *I–V* measurement. Pt is one of less reactive metals and less likely to be oxidized than Al. As can be seen from Fig. 6, tristable conductance switching behavior was also obtained *via* ITO/**DPAPIT**/C-AFM tip device. In addition, the possibility of the diffusion of Pt atoms into the azo film as the deep charge trapping site may be excluded because the top electrode of the sandwich memory device was just the Pt tip directly top-contact to the organic thin layer instead of vapor-deposition process. Therefore, the clear switching behavior of small molecule films using different electrode materials could rule out the possibility of filament conduction. The proposed electrical switching mechanism of the fabricated devices based on **DPAPIT** can be explained as below. DFT molecular simulation results (Fig. 7a) showed that an open channel is formed from the molecular surface throughout the conjugated backbone with continuous positive molecular electrostatic potential (ESP, in red), through which charge carriers can migrate. The negative ESP regions (in blue) caused by the electron-deficient groups, such as azobenzene chromophore and phthalimide moiety, can function as "traps" to reduce the mobility of the charge carriers.[42,43] The depth of these traps is in accordance with the electron-withdrawing ability of the functional groups listed above. Due to the highly ordered crystalline thin-films, all the traps in the molecules have equal opportunities to accept the injected charge carriers. The shallower electron traps arising from the *azo* group will be filled quickly, leading to the current transition from OFF to the ON1 state. The deeper charge traps arising from the phthalimide moiety will be filled later, resulting in the current transition from the ON1 to ON2 state. The HOMO and LUMO surfaces of **DPAPIT** are shown in Fig. 7b. Upon the HOMO to LUMO transition, the electron density shifts from the donor to acceptor side and becomes more localized. Moreover, the trapped charge carriers were stabilized by intramolecular charge transfer which could form a charge-separated state. The trapped electrons may not be easily detrapped under non-degrading reverse fields, resulting in a high conductivity state that can be maintained for a long time. Accordingly, the device shows a WORM-type characteristic.

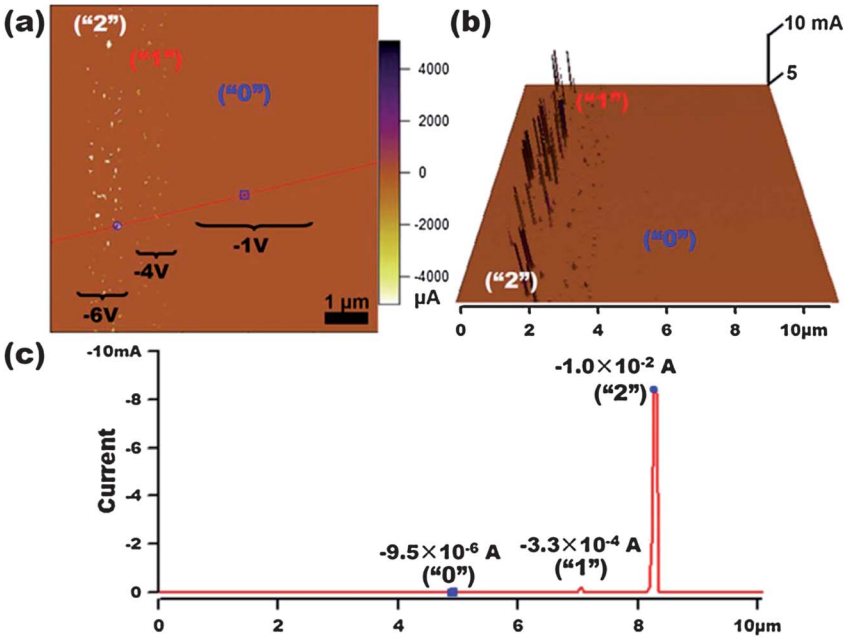

Fig. 6 C-AFM image of **DPAPIT** film vacuum-deposited onto ITO substrate. (a) After successively applying −1 V, −4 V and −6 V voltage pulses at different areas of the film, the scan area is 10 μm × 10 μm; (b) 3D C-AFM image of (a), the low-to-high changes of the height of the current peaks represent "0", "1" and "2" tri-stable states, respectively; (c) cross-section profile shows the current intensity in (a) at different written areas.

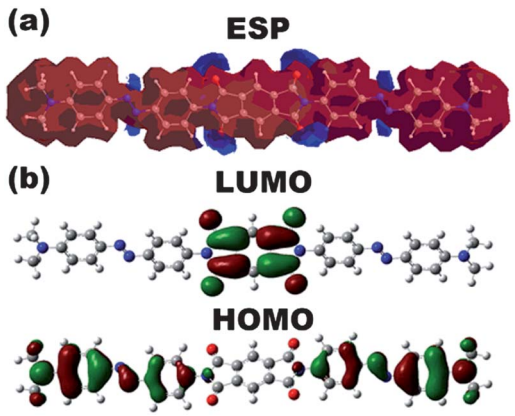

Fig. 7 DFT molecular simulation results (B3LYP/6-311G (d) level) of **DPAPIT**: (a) molecular electrostatic potential (ESP) surfaces; (b) HOMO and LUMO.

Conclusions

In summary, two small molecules containing the same electron-rich and electron-deficient moieties with different molecular length were synthesized and fabricated as the electroactive layers of the sandwich-structure memory devices. The long molecule **DPAPIT** stacked closely in the thin film during the vacuum-deposition and annealing process, resulting in high-performance nonvolatile ternary data storage devices. Whereas the short molecule film was amorphous and the memory devices showed no obvious conductance switching behaviour. The molecular length, morphology, and annealing temperature are identified to play vital roles in the memory device performance. In addition, the crystallinity and surface roughness of **DPAPIT** thin films were significantly improved as the annealing temperature increased, leading to the low operating voltages which are highly desirable for low-power comsumption data-storage devices. The first realization of the writing and reading of ternary data storage signals at a nanoscale thin-film by using C-AFM is relatively significant in terms of miniaturization of ternary data storage devices. We hope that these results discussed here could provide guidance for the design and synthesis of more superior materials for future UHDDS applications.

Acknowledgements

This work was supported by the Chinese Natural Science Foundation (NSFC 21076134, 21176164), the Natural Science Foundation of Jiangsu Province (BK2010208), and the Doctoral Program of Higher Education of China (Grant no. 20113201130003). We sincerely thank professor Qing-Hua Xu for some beneficial discussion and revision of this work.

Notes and references

1 (*a*) R. Hagen and T. Bieringer, *Adv. Mater.*, 2001, **13**, 1805–1810; (*b*) S. Kawata and Y. Kawata, *Chem. Rev.*, 2000, **100**, 1777–1788.
2 M. Emmelius, G. Pawlowski and H. Vollmann, *Angew. Chem., Int. Ed. Engl.*, 1989, **28**, 1445–1471.
3 J. P. Wang, *Nat. Mater.*, 2005, **4**, 191–192.
4 T. Osaka, M. Takai, K. Hayashi, K. Ohashi, M. Saito and K. Yamada, *Nature*, 1998, **392**, 796–798.
5 (*a*) S. R. Forrest, *Nature*, 2004, **428**, 911–918; (*b*) J. C. Scott, *Science*, 2004, **304**, 62–63; (*c*) J. C. Scott and L. D. Bozano, *Adv. Mater.*, 2007, **19**, 1452–1463.
6 (*a*) Y. Yonekuta, K. Susuki, K. Oyaizu, K. Honda and H. Nishide, *J. Am. Chem. Soc.*, 2007, **129**, 14128–14129; (*b*) T. Iimori, T. Naito and N. Ohta, *J. Am. Chem. Soc.*, 2007, **129**, 3486–3487; (*c*) X.-D. Zhuang, Y. Chen, B.-X. Li, D.-G. Ma, B. Zhang and Y. Li, *Chem. Mater.*, 2010, **22**, 4455–4461; (*d*) D. I. Son, T. W. Kim, J. H. Shim, J. H. Jung, D. U. Lee, J. M. Lee, W. I. Park and W. K. Choi, *Nano Lett.*, 2010, **10**, 2441–2447.

7 (*a*) Q.-D. Ling, D.-J. Liaw, C. Zhu, D. S.-H. Chan, E.-T. Kang and K.-G. Neoh, *Prog. Polym. Sci.*, 2008, **33**, 917–978; (*b*) Q.-D. Ling, D.-J. Liaw, E. Y.-H. Teo, C. Zhu, D. S.-H. Chan, E.-T. Kang and K.-G. Neoh, *Polymer*, 2007, **48**, 5182–5201; (*c*) Q.-D. Ling, Y. Song, S.-L. Lim, E. Y.-H. Teo, Y.-P. Tan, C. Zhu, D. S. H. Chan, D.-L. Kwong, E.-T. Kang and K.-G. Neoh, *Angew. Chem., Int. Ed.*, 2006, **45**, 2947–2951; (*d*) Q. D. Ling, F. C. Chang, Y. Song, C. X. Zhu, D. J. Liaw, D. S. H. Chan, E. T. Kang and K. G. Neoh, *J. Am. Chem. Soc.*, 2006, **128**, 8732–8733.

8 (*a*) L. H. Xie, Q. D. Ling, X. Y. Hou and W. Huang, *J. Am. Chem. Soc.*, 2008, **130**, 2120–2121; (*b*) J. Liu, Z. Yin, X. Cao, F. Zhao, A. Lin, L. Xie, Q. Fan, F. Boey, H. Zhang and W. Huang, *ACS Nano*, 2010, **4**, 3987–3992.

9 (*a*) J. Lee, H. Chang, S. Kim, G. S. Bang and H. Lee, *Angew. Chem., Int. Ed.*, 2009, **48**, 8501–8504; (*b*) J. Lee, E. Lee, S. Kim, G. S. Bang, D. A. Shultz, R. D. Schmidt, M. D. E. Forbes and H. Lee, *Angew. Chem., Int. Ed.*, 2011, **50**, 4414–4418.

10 S. C. Choi, S. H. Hong, S. H. Cho, S. Park, S. M. Park, O. Kim and M. Ree, *Adv. Mater.*, 2008, **20**, 1766–1771.

11 A. Bandyopadhyay and A. J. Pal, *Adv. Mater.*, 2003, **15**, 1949–1952.

12 J. Ouyang, C.-W. Chu, C. R. Szmanda, L. Ma and Y. Yang, *Nat. Mater.*, 2004, **3**, 918–922.

13 C. W. Chu, J. Ouyang, J.-H. Tseng and Y. Yang, *Adv. Mater.*, 2005, **17**, 1440–1443.

14 (*a*) S. G. Hahm, S. Choi, S.-H. Hong, T. J. Lee, S. Park, D. M. Kim, W.-S. Kwon, K. Kim, O. Kim and M. Ree, *Adv. Funct. Mater.*, 2008, **18**, 3276–3282; (*b*) S. Baek, D. Lee, J. Kim, S.-H. Hong, O. Kim and M. Ree, *Adv. Funct. Mater.*, 2007, **17**, 2637–2644.

15 (*a*) Y. Li, H. Xu, X. Tao, K. Qian, S. Fu, Y. Shen and S. Ding, *J. Mater. Chem.*, 2011, **21**, 1810–1821; (*b*) V. Meded, A. Bagrets, A. Arnold and F. Evers, *Small*, 2009, **5**, 2218–2223.

16 J.-C. Hsu, C.-L. Liu, W.-C. Chen, K. Sugiyama and A. Hirao, *Macromol. Rapid Commun.*, 2011, **32**, 528–533.

17 X.-D. Zhuang, Y. Chen, G. Liu, P.-P. Li, C.-X. Zhu, E.-T. Kang, K.-G. Noeh, B. Zhang, J.-H. Zhu and Y.-X. Li, *Adv. Mater.*, 2010, **22**, 1731–1735.

18 (*a*) Y. Ma, X. Cao, G. Li, Y. Wen, Y. Yang, J. Wang, S. Du, L. Yang, H. Gao and Y. Song, *Adv. Funct. Mater.*, 2010, **20**, 803–810; (*b*) G. Jiang, Y. Song, X. Guo, D. Zhang and D. Zhu, *Adv. Mater.*, 2008, **20**, 2888–2898; (*c*) Y. Shang, Y. Wen, S. Li, S. Du, X. He, L. Cai, Y. Li, L. Yang, H. Gao and Y. Song, *J. Am. Chem. Soc.*, 2007, **129**, 11674–11675; (*d*) H. Wu, Y. Song, S. Du, H. Liu, H. Gao, L. Jiang and D. Zhu, *Adv. Mater.*, 2003, **15**, 1925–1929; (*e*) N.-H. You, C.-C. Chueh, C.-L. Liu, M. Ueda and W.-C. Chen, *Macromolecules*, 2009, **42**, 4456–4463.

19 S. L. Lim, N.-J. Li, J.-M. Lu, Q.-D. Ling, C. X. Zhu, E.-T. Kang and K. G. Neoh, *ACS Appl. Mater. Interfaces*, 2009, **1**, 60–71.

20 (*a*) W. L. Kwan, R. J. Tseng, W. Wu, Q. Pei and Y. Yang, *IEEE Int. Electron Devices Meet., Tech. Dig., 50th*, 2007, 237; (*b*) M. Caironi, D. Natali, E. Canesi, A. Bianco, C. Bertarelli, G. Zerbi and M. Sampietro, *Thin Solid Films*, 2008, **516**, 7680–7684; (*c*) H.-T. Lin, Z. Pei, J.-R. Chen, C.-P. Kung, Y.-C. Lin, C.-M. Tseng and Y.-J. Chan, *IEEE Int. Electron Devices Meet., Tech. Dig., 50th*, 2007, 233; (*d*) T.-W. Kim, H. Choi, S.-H. Oh, G. Wang, D.-Y. Kim, H. Hwang and T. Lee, *Adv. Mater.*, 2009, **21**, 2497–2500; (*e*) B. Cho, S. Song, Y. Ji, T.-W. Kim and T. Lee, *Adv. Funct. Mater.*, 2011, **21**, 2806–2829.

21 Y. W. Jung, S. H. Lee, A. T. Jennings and R. Agarwal, *Nano Lett.*, 2008, **8**, 2056–2062.

22 H. Li, Q. Xu, N. Li, R. Sun, J. Ge, J. Lu, H. Gu and F. Yan, *J. Am. Chem. Soc.*, 2010, **132**, 5542–5543.

23 S. Loser, C. J. Bruns, H. Miyauchi, R. P. Ortiz, A. Facchetti, S. I. Stupp and T. J. Marks, *J. Am. Chem. Soc.*, 2011, **133**, 8142–8145.

24 (*a*) A. Facchetti, M.-H. Yoon, C. L. Stern, H. E. Katz and T. J. Marks, *Angew. Chem., Int. Ed.*, 2003, **42**, 3900–3903; (*b*) D. H. Kim, D. Y. Lee, H. S. Lee, W. H. Lee, Y. H. Kim, J. I. Han and K. Cho, *Adv. Mater.*, 2007, **19**, 678–682.

25 (*a*) D. Jurchescu, S. Subramanian, R. J. Kline, S. D. Hudson, J. E. Anthony, T. N. Jackson and D. J. Gundlach, *Chem. Mater.*, 2008, **20**, 6733–6737; (*b*) K. H. Kim, S. Y. Bae, Y. S. Kim, J. A. Hur, M. H. Hoang, T. W. Lee, M. J. Cho, Y. Kim, M. Kim, J.-I. Jin, S.-J. Kim, K. Lee, S. J. Lee and D. H. Choi, *Adv. Mater.*, 2011, **23**, 3095–3102.

26 (*a*) G. Qian, Z. Zhong, M. Luo, D. Yu, Z. Zhang, Z. Y. Wang and D. Ma, *Adv. Mater.*, 2009, **21**, 111–116; (*b*) C. Han, G. Xie, H. Xu, Z. Zhang, L. Xie, Y. Zhao, S. Liu and W. Huang, *Adv. Mater.*, 2011, **23**, 2491–2496.

27 (*a*) L.-S. Liao, W. K. Slusarek, T. K. Hatwar, M. L. Ricks and D. L. Comfort, *Adv. Mater.*, 2008, **20**, 324–329; (*b*) L. S. Liao and C. W. Tang, *J. Appl. Phys.*, 2008, **104**, 044501.

28 (*a*) D. G. Patel, N. M. Bastianon, P. Tongwa, J. M. Leger, T. V. Timofeeva and G. P. Bartholomew, *J. Mater. Chem.*, 2011, **21**, 4242–4250; (*b*) J. Mei, K. R. Graham, R. Stalder, S. P. Tiwari, H. Cheun, J. Shim, M. Yoshio, C. Nuckolls, B. Kippelen, R. K. Castellano and J. R. Reynolds, *Chem. Mater.*, 2011, **23**, 2285–2288.

29 M. Riede, C. Uhrich, J. Widmer, R. Timmreck, D. Wynands, G. Schwartz, W.-M. Gnehr, D. Hildebrandt, A. Weiss, J. Hwang, S. Sudharka, P. Erk, M. Pfeiffer and K. Leo, *Adv. Funct. Mater.*, 2011, **21**, 3019–3028.

30 (*a*) O. P. Lee, A. T. Yiu, P. M. Beaujuge, C. H. Woo, T. W. Holcombe, J. E. Millstone, J. D. Douglas, M. S. Chen and J. M. J. Fréchet, *Adv. Mater.*, 2011, **23**, 5359–5363; (*b*) S. Fabiano, H. Wang, C. Piliego, C. Jaye, D. A. Fischer, Z. Chen, B. Pignataro, A. Facchetti, Y.-L. Loo and M. A. Loi, *Adv. Funct. Mater.*, 2011, **21**, 4479–4486.

31 H. Hoppe and N. S. Sariciftci, *J. Mater. Chem.*, 2006, **16**, 45–61.

32 S. Yagai, T. Nakajima, T. Karatsu, K. Saitow and A. Kitamura, *J. Am. Chem. Soc.*, 2004, **126**, 11500–11508.

33 (*a*) Y. Zhou, M. Xu, J. Wu, T. Yi, J. Han, S. Xiao, F. Li and C. Huang, *J. Phys. Org. Chem.*, 2008, **21**, 338–343; (*b*) B.-C. Yu, Y. Shirai and J. M. Tour, *Tetrahedron*, 2006, **62**, 10303–10310.

34 J. Shi, Z. Jiang and S. Cao, *React. Funct. Polym.*, 2004, **59**, 87–91.

35 M. Hagiri, N. Ichinose, C. Zhao, H. Horiuchi, H. Hirtasuka and T. Nakayama, *Chem. Phys. Lett.*, 2004, **391**, 297–301.

36 Y. Shang, Y. Wen, S. Li, S. Du, X. He, L. Cai, Y. Li, L. Yang, H. Gao and Y. Song, *J. Am. Chem. Soc.*, 2007, **129**, 11674–11675.

37 M. Surin, P. Sonar, A. C. Grimsdale, K. Müllen, S. De Feyter, S. Habuchi, S. Sarzi, E. Braeken, A. V. Heyen, M. Van der Auweraer, F. C. De Schryver, M. Cavallini, J. F. Moulin, F. Biscarini, C. Femoni, L. Roberto and P. Leclère, *J. Mater. Chem.*, 2007, **17**, 728–735.

38 R. Schmidt, J. H. Oh, Y.-S. Sun, M. Deppisch, A.-M. Krause, K. Radacki, H. Braunschweig, M. Könemann, P. Erk, Z. Bao and F. Würthner, *J. Am. Chem. Soc.*, 2009, **131**, 6215–6228.

39 J. H. Oh, S. Liu, Z. Bao, R. Schmidt and F. Würthner, *Appl. Phys. Lett.*, 2007, **91**, 212107.

40 R. J. Chesterfield, J. C. McKeen, C. R. Newman, P. C. Ewbank, D. A. da Silva, J. L. Bredas, L. L. Miller, K. R. Mann and C. D. Frisbie, *J. Phys. Chem. B*, 2004, **108**, 19281–19292.

41 (*a*) W. L. Kwan, B. Lei, Y. Shao, S. V. Prikhodko, N. Bodzin and Y. Yang, *J. Appl. Phys.*, 2009, **105**, 124516–124520; (*b*) B. Lei, W. L. Kwan, Y. Shao and Y. Yang, *Org. Electron.*, 2009, **10**, 1048–1053; (*c*) F. Verbakel, S. C. J. Meskers, R. A. J. Janssen, H. L. Gomes, M. Cölle, M. Büchel and D. M. de Leeuw, *Appl. Phys. Lett.*, 2007, **91**, 192103; (*d*) M. Cölle, M. Büchel and D. M. de Leeuw, *Org. Electron.*, 2006, **7**, 305–312.

42 X.-D. Zhuang, Y. Chen, G. Liu, B. Zhang, K.-G. Neoh, E.-T. Kang, C.-X. Zhu, Y.-X. Li and L.-J. Niu, *Adv. Funct. Mater.*, 2010, **20**, 2916–2922.

43 G. Liu, B. Zhang, Y. Chen, C.-X. Zhu, L. Zeng, D. S.-H. Chan, K.-G. Neoh, J. Che and E.-T. Kang, *J. Mater. Chem.*, 2011, **21**, 6027–6033.